Mon. Not. R. Astron. Soc. **362,** 1054–1064 (2005) doi:10.1111/j.1365-2966.2005.09373.x

Stellar populations and Lyα emission in two lensed $z \gtrsim 6$ galaxies

Daniel Schaerer[1,2]★ and Roser Pelló[2]

[1]*Observatoire de Genève, 51, Ch. des Maillettes, CH-1290 Sauverny, Switzerland*

[2]*Laboratoire d'Astrophysique (UMR 5572), Observatoire Midi-Pyrénées, 14 Avenue E. Belin, F-31400 Toulouse, France*

Accepted 2005 June 28. Received 2005 June 28; in original form 2005 January 5

ABSTRACT

We present an analysis of two strongly lensed galaxies at $z = 6.56$ and $z \sim 7$ for which multi-band photometric and spectroscopic observations are available. For one source, the data include recent *Hubble Space Telescope* (*HST*) and *Spitzer* observations. Using a spectral energy distribution (SED) fitting technique considering a number of parameters (various libraries of empirical and theoretical template spectra, variable extinction and extinction laws), we attempt to constrain the properties of their stellar populations (age, star formation (SF) history and mass) and their intrinsic Lyman α (Lyα) emission. The following main results are obtained for the individual galaxies.

(i) Triple arc in Abell 2218, probable $z \sim 7$ galaxy. The most likely redshift of this source is $z \sim 6.0$–7.2, taking into account both our photometric determination and lensing considerations. SED fits indicate generally a low extinction [$E(B-V) \lesssim 0.05$], but do not strongly constrain the SF history. Best fits have typical ages of ∼3–400 Myr. A reasonable maximum age of 250–650 Myr (1σ interval) can be estimated. However, the apparent 4000-Å break observed recently from the combination of (Infrared Array Camera) IRAC/*Spitzer* and *HST* observations can also be reproduced equally well with the template of a young (∼3–5 Myr) burst where strong rest-frame optical emission lines enhance the 3.6- and 4.5-μm fluxes. The estimated star formation rate (SFR) is typically ∼1 $M_\odot$ yr^{-1} for a Salpeter initial mass function (IMF) from 1 to 100 $M_\odot$, in agreement with previous estimates. The unknowns on the age and SF history could easily explain the apparent absence of Lyα in this galaxy.

(ii) Abell 370 HCM 6A. The available Lyα and continuum observations indicate basically two possible solutions: (1) a young burst or ongoing constant SF with non-negligible extinction or (2) a composite young + 'old' stellar population. In the first case, one obtains a best fit, $E(B-V) \sim 0.25$, or $A_V \sim 0.5$–1.8 at a 1σ level. In consequence, we obtain SFR ∼11–41 $M_\odot$ yr^{-1}, higher than earlier estimates, and we estimate a fairly high total luminosity [$L \sim (1-4) \times 10^{11}$ $L_\odot$] for this galaxy, in the range of luminous infrared galaxies. A Lyα transmission of ∼23–90 per cent is estimated from our best-fitting models. Other properties (age and SF history) remain largely unconstrained. In case of composite stellar populations, the SFR, mass and luminosity estimate are lower. The two scenarios may be distinguishable with IRAC/*Spitzer* observations at 3.6 and 4.5 μm.

Key words: galaxies: evolution – galaxies: high-redshift – galaxies: starburst – early Universe – infrared: galaxies.

1 INTRODUCTION

Little is known about the stellar properties, extinction and the expected intrinsic Lyman α (Lyα) emission of distant, high-redshift galaxies. Indeed, although it has in the recent past become possible through various techniques to detect already sizeable numbers of galaxies at $z \gtrsim 5$ (see e.g. the reviews of Taniguchi et al. 2003; Spinrad 2003), the information available on these objects remains generally scant. For example, in many cases the galaxies are just detected in two photometric bands and Lyα line emission, when present, serves to determine the spectroscopic redshift (e.g. Bremer et al. 2004; Bunker et al. 2004; Dickinson et al. 2004). Then the photometry is basically used to estimate the star formation rate (SFR) assuming standard conversion factors between the ultraviolet (UV)

★E-mail: daniel.schaerer@obs.unige.ch

rest-frame light and the SFR, and nothing is known about the extinction and the properties of the stellar population (such as age, detailed star formation (SF) histories, etc.).

At higher redshift ($z \gtrsim 6$), even less information is generally available (but see a recent study of Eyles et al. 2005 on two $z \sim 6$ galaxies observed with *HST* and *Spitzer*). Many objects are found by Lyα emission, but remain weak or sometimes even undetected in the continuum (e.g. Rhoads & Malhotra 2001; Ajiki et al. 2003; Cuby et al. 2003; Kodaira et al. 2003; Taniguchi et al. 2005). In these cases, the Lyα luminosity can be determined and used to estimate an SFR using again standard conversion factors. Also the Lyα equivalent width is estimated, providing some possible clue on the nature of these sources. However, this has led to puzzling results, for example, for the sources from the Large Area Lyman α (LALA) survey, which seem to show unusually large Lyα equivalent widths that are difficult to understand without invoking exceptional conditions (Pop III stars?; Malhotra & Rhoads 2002; Rhoads et al. 2003). Given the few data available for the LALA sources, it is fair to say that the nature of these objects, their stellar populations, extinction, etc. remain currently largely unknown (cf. Dawson et al. 2004). When possible, a simple comparison between the UV and Lyα SFR is undertaken providing possibly information on the Lyα transmission, that is, the partial absorption of Lyα photons on their sight line through the intergalactic medium (IGM: e.g. Haiman 2002; Santos 2004) and/or on partial Lyα 'destruction' processes close to the source [e.g. due to dust or interstellar medium (ISM) geometry; Charlot & Fall 1993; Valls-Gabaud 1993; Tenorio-Tagle et al. 1999; Mas-Hesse et al. 2003].

Notable exceptions of $z \gtrsim 4$ samples for which some estimate of extinction is available from multi-band photometry, include work on the Subaru Deep Survey (Ouchi et al. 2004) and *Great Observatories Origins Deep Survey* (*GOODS*) data (e.g. Papovich et al. 2004). Lehnert & Bremer (2004) also discuss some preliminary information on small amounts of extinction in their $z > 5$ sources. Interestingly, in their study of a $z = 5.34$ galaxy discovered by Dey et al. (1998), Armus et al. (1998) find indications for significant reddening ($A_V > 0.5$ mag) from the analysis of the observed SED and from the presence of Lyα emission.

In a similar manner, we will here present a consistent study of the stellar population properties, extinction and the Lyα emission for two galaxies at redshift $z \gtrsim 6$. For this aim, we use two distant ($z \gtrsim 6$) gravitationally lensed galaxies for which multi-band photometry is available (detection in at least three to four bands). Through a quantitative analysis of their SEDs, using a vast library of empirical and theoretical template spectra, we aim to constrain properties of the stellar populations, such as age and SF history (burst or constant SF?) and their extinction. Furthermore by comparing the Lyα emission expected from the stellar population constraint with the observed Lyα flux, we estimate consistently the Lyα 'transmission' for the individual sources.

The Lyα transmission and SF properties derived here can in principle be used to infer the ionization fraction of hydrogen in the IGM at a given redshift (cf. Haiman 2002; Santos 2004), a key quantity of interest for the study of the reionization history of the Universe (cf. review from Barkana & Loeb 2001). Obviously, the present 'exploratory' work will have to be extended to larger galaxy samples, and sophisticated tools will probably be needed to interpret such results in terms of IGM properties (cf. Gnedin & Prada 2004). However, this approach should be complementary to other methods probing the reionization history by measuring the Gunn–Peterson optical depth observed in quasar spectra as a function of redshift (e.g. Becker et al. 2001; Fan et al. 2003), or by comparing Lyα luminosity functions at different redshifts (e.g. Malhotra & Rhoads 2004).

The remainder of this paper is structured as follows. In Section 2, we summarize the adopted observational constraints from the literature. Our modelling technique is described in Section 3. The detailed results for each galaxy are presented in Sections 4 and 5. Our main conclusions are summarized in Section 6.

2 OBSERVATIONAL CONSTRAINTS

The two galaxies studied here are: (i) the probable $z \sim 7$ galaxy recently discovered by Kneib et al. (2004, hereafter KESR), which presently lacks a spectroscopic redshift, but for which rather accurate multi-band *HST* observations are available, allowing us in particular also to derive a fairly reliable photometric redshift; and (ii) the $z = 6.56$ Lyα emitter HCM 6A behind the lensing cluster Abell 370. We now summarize the observational data, taken from the literature. The adopted redshift and gravitational magnification factors are listed in Table 1.

Before proceeding, let us mention for clarity that these two objects are generally considered to be star-forming galaxies (starbursts), not active galactic nuclei (AGN) (narrow line – type II – or others), as no contradicting information is available so far. However, one must bear in mind that some of the interpretations presented below (and in the literature) may need to be revised, should this assumption be incorrect.

Triple arc in Abell 2218. The observational data for this object, named Abell 2218 KESR hereafter, are taken from KESR and from Egami et al. (2005). The photometry from KESR includes observations with *HST* (WFPC2, ACS and NICMOS) in V_{606W}

Table 1. Summary of the main adopted and estimated properties of the analysed high redshift galaxies. The adopted magnification μ is given in column 2, column 3 gives the redshift, column 4 gives an indication on the most plausible SF history (burst or constant SF), column 5 gives a plausible age of the stellar population, column 6 gives an estimate of the optical extinction A_V (for the Calzetti et al. 2000 law), column 7 gives the estimated SFR (for a Salpeter IMF from 1 to 100 $M_\odot$), column 8 gives an estimated stellar mass (for same IMF), column 9 gives the estimated bolometric luminosity and column 10 gives the estimated Lyα transmission (fraction of intrinsic emitted flux over observed Lyα flux). See Figs 5 and 7 and the corresponding text for an estimate of the confidence levels and the range of parameters.

Object	μ	Redshift	SF history	Age (Myr)	A_V (mag)	SFR ($M_\odot$ yr^{-1})	Stellar mass ($M_\odot$)	L_{bol} ($L_\odot$)	Lyα transmission
Abell 2218 KESR	25	∼6.0–7.2	?	3–400	Negligible?	∼1	(0.3–6) × 10^8	∼2 × 10^{10}	
Abell 370 HCM6A	4.5	6.56	CSFR/ young burst	?	∼1	11–41	(1–4) × 10^8	(1–4) × 10^{11}	23–90 per cent
			Composite	Young+'old'	Negligible	>0.4–0.8	∼2 × 10^9	∼3 × 10^{10}	≳40 per cent

(undetected), I_{814W}, z_{850LP} and H_{160W}, and with NIRC/Keck in J. Subsequently, additional photometry was obtained with NICMOS/*HST* in the J band (F110W), and with IRAC/*Spitzer* at 3.6 and 4.5 μm (see Egami et al. 2005) For our computations (see below), we have used the appropriate filter transmission curves. In particular, updated transmission curves were used for the ACS and NICMOS filters (M. Sirianni, private communication; Sirianni et al. 2004; R. Thompson, private communication).

Few brief comments concerning the photometry are needed here. First, KESR present photometry for two multiple images (a and b). Apparently, sources a and b differ in the z_{850LP} flux (with quoted errors of ± 0.05 mag) by 3.2σ, whereas the fluxes in the other filters agree well within 1σ. Differential lensing across the images together with sampling effects could be responsible for this small discrepancy. As we are interested in a global representative SED for this source, we have chosen to use the averaged photometric SED, the magnification factors being the same for the two images. Finally, we have also noted some apparent discrepancies between the measurements reported in KESR and Egami et al. (2005), the most important one being the H_{160W} flux, which is ∼15–20 per cent (3–4σ) higher in the latter publication. These differences are mostly due to the use of different apertures on different repixeled/rescaled images (J. Richard, private communication). Again, this illustrates the difficulty in deriving reliable colours for extended arcs. To account for these small discrepancies and for the possible error underestimate, we therefore adopt a minimum photometric error of 0.15 mag in all filters. It is worth noting that photometric errors translate into absolute flux calibration errors for fitting purposes. As we will see below, adopting the latter minimum error bars significantly improves the SED fits.

In addition to the photometry, the non-detection of the source with Keck LRIS spectroscopy provides an upper limit on the continuum flux between 9000 and 9300 Å (KESR). This upper limit will be used as an additional constraint in our SED modelling. KESR also indicate a possible drop of the continuum below ∼9800 Å from their Keck II NIRSPEC spectrum. For various reasons, the reality of this spectral break is questionable. First, a true neutral hydrogen break ('Lyα break') at ∼9800 Å, far in the red wing of the z_{850LP} filter, seems incompatible with the relatively strong flux measured in this filter. Furthermore, test computations show that such a break is difficult if not impossible to reconcile with our spectral modelling. In any case, the significance of this finding appears questionable as the detected continuum is extremely faint and noisy. The reality of this spectral feature is now also questioned by Egami et al. (2005). For these reasons this information is discarded from our spectral fitting.

In practice, we have retained the following two variants to describe the observed SED of this source: (SED1) the average fluxes (I_{814W}, z_{850LP}, H_{110W} and H_{160W}) of images a and b from KESR plus the IRAC/*Spitzer* data of image b from Egami et al.; and (SED2) all fluxes from image b from Egami et al. These are treated as SEDs from two different objects. Furthermore, for each of these 'objects', we have computed two cases in our SED fitting described below: (i) the observed SEDs in I_{814W}, z_{850LP}, H_{110W}, H_{160W}, 3.6 and 4.5 μm; and (ii) same as (i) plus the flux limits from the V_{606W} and Keck LRIS non-detections.

No emission line has so far been detected for Abell 2218 KESR. Its spectroscopic redshift remains therefore presently unknown, but the well-constrained mass model for the cluster strongly suggests a redshift $z \gtrsim 6$ for this source (KESR, Egami et al. 2005). The magnification factors of both the images a and b are $\mu = 25 \pm 3$, according to KESR.

Abell 370 HCM6A. The observational data of this $z = 6.56$ galaxy are taken from Hu et al. (2002). The photometry includes *VRIZJHK′* from Keck I and II (LRIS and Echellette Spectrograph and Imager) and from Subaru (CISCO/OHS). The gravitational magnification of the source is $\mu = 4.5$ according to Hu et al. (2002).

Photometric fluxes and errors were adopted from their fig. 3. Where possible the appropriate filter transmission curves were used. The '*Z*'-band filter transmission is somewhat uncertain, as these observations were undertaken using an RG850 filter, which together with the LRIS optics and the CCD response, yields a transmission similar to a *Z*-band filter (Hu, McMahon & Cowie 1999). Our approximate filter curve shows a blueward shift of $\lambda_{\rm eff}$ by ∼200 Å compared to the information given by Hu et al. (1999). However, since the redshift is known for this source and since we adjust the observed flux (not magnitude) in this band, this should not affect our conclusions.

3 SED MODELLING

3.1 Main rest-frame UV-optical SED features of high-*z* galaxies and their 'information content'

Before proceeding to the fits of the individual SEDs, a brief comment on the available SED features seems appropriate.

For obvious reasons, the available SED (basically from broad-band photometry) of high-z ($z \gtrsim 6$) galaxies is primarily limited to the rest-frame UV (when observed from the ground) or optical spectrum (when available e.g. with *Spitzer* and future satellite missions). The main information 'encoded' in this SED is therefore: (1) the neutral H I break shortward of Lyα (the 'Lyα' break) due to the strong or complete Gunn–Peterson trough; (2) the slope of the UV spectrum and (3) possibly a 4000-Å break (hereafter denoted Balmer break), if present and covered by the observations. In addition, the presence of the Lyα line, mostly used to determine spectroscopically the redshift, provides clear evidence for ongoing massive SF.

The position of the Lyα break depends essentially on redshift. The UV slope depends on the intrinsic spectrum – in turn depending mostly on age and SF history – and on the extinction, that is, the extinction law and the amount of reddening. The Balmer break becomes visible (in absorption) in the continuum of stellar populations after $\gtrsim$10–30 Myr. Lyα emission, if due to stellar photoionization and not AGN activity, indicates the presence of young ($\lesssim$10 Myr) massive ionizing stars.

Concerning the UV slope, it is useful to recall that this quantity[1] does not lend itself to determine the metallicity of a star-forming galaxy from a theoretical point of view and in terms of individual objects. The reasons are that, intrinsically, the UV slope shows only small variations with metallicity, and that the slope depends strongly on the exact SF history (see e.g. Leitherer & Heckman 1995; Meurer et al. 1995). This is illustrated in Fig. 1 where β (measured over the interval 1300–1800 Å) is plotted as a function of age for populations of metallicities between solar and zero (PopIII) and for the limiting cases of bursts and SFR = constant. Furthermore, as pointed out in Schaerer (2002, 2003) and also shown in this figure, for very low metallicities ($Z \lesssim 1/50\,Z_\odot$), nebular continuous emission becomes dominant even down to UV wavelengths (longward of Lyα), such

[1] Various definitions of the UV slope exist. The most commonly used ones, generally denoted by β, are defined as the power-law index of the SED in F_λ versus λ over a certain wavelength interval.

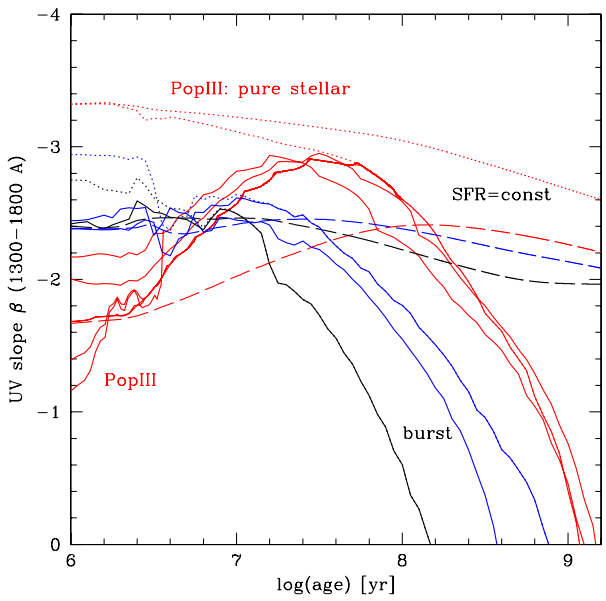

Figure 1. Temporal evolution of the UV slope β measured between 1300 and 1800 Å from synthesis models of different metallicities and for instantaneous bursts (solid lines) and constant SF (long dashed lines). Black lines show solar metallicity models, red lines show metallicities between $Z = 10^{-5}$ and zero (PopIII) and blue lines show intermediate cases of $Z = 0.004$ and 0.0004. The dotted lines show β if nebular continuous emission is neglected, that is, assuming pure stellar emission. Note especially the strong degeneracies of β in age and metallicity for bursts, the insensitivity of β on Z for constant SF, and the rather red slope for young very metal-poor bursts. Further discussions in the text.

that the observed integrated (stellar+nebular) spectrum has even a flatter UV slope than high metallicity starbursts. In other words, even for bursts, there are strong intrinsic degeneracies of β between age and metallicity, to which the additional effect of reddening must be added, including the uncertainties on the a priori unknown extinction law. It is therefore evident that on an individual object basis there are in general degeneracies between age, metallicity, SF history and extinction. However, this does not preclude the possible existence of statistical correlations between quantities such as, for example, β and metallicity in large samples of galaxies, as known to hold, for example, for local UV selected starbursts (cf. Heckman et al. 1998). Also, as we will see below, there are cases where the UV slope and the mere fact of the presence of an emission line allow us nevertheless to lift some degeneracies and therefore to determine interesting constraints on the stellar population and on extinction.

The behaviour of the 4000-Å break and its use as an age indicator have extensively been discussed in the literature (e.g. Bruzual 1983 and recently Kauffmann et al. 2003). As in simple stellar populations, its amplitude is basically a monotonically increasing function of age, an estimate of the break, for example, obtained from 3.8 to 4.5 μm photometry with IRAC/*Spitzer* and *JHK* photometry in $z \gtrsim 6$ galaxies, provides information on the age of the light-emitting stellar population. Since the exact SF history cannot be determined in these cases (in contrast to studies at low z, cf. Kauffmann et al. 2003), the amplitude of the break provides a range of ages, the minimum age being given by instantaneous bursts and the maximum age from models with constant SF. For obvious reasons this maximum 'luminosity weighted' age derived from a measure of the Balmer break is also unaffected by the considerations of possible multiple stellar populations. The same is not true for the minimum age, which is, however, of less cosmological interest.

3.2 Spectral fitting

For the spectral fitting, we use a slightly adapted version of the photometric redshift code HYPERZ of Bolzonella, Miralles & Pelló (2000). HYPERZ does standard SED fitting using a number of modelling parameters. The free parameters for the SED modelling are:

(i) the spectral template;
(ii) extinction and the reddening law; and
(iii) a parameter $f_{\rm Lyf}$ describing possible deviations from the average Lyman-forest attenuation from Madau (1995).

For Abell 2218 KESR, the source redshift is also a free parameter.

For the spectral templates, we use a large compilation of empirical and theoretical SEDs, including starbursts, quasi-stellar object (QSO) and galaxies of all Hubble types, and covering various SF histories (bursts, exponentially decreasing and constant SF) and various metallicities. For most applications, we group the templates in the following way.

(i) **Starbursts and QSOs (hereafter SB+QSO)**: this group includes the starburst templates with $E(B-V)$ from <0.1 to 0.7 from the Calzetti, Kinney & Storchi-Bergmann (1994) and Kinney et al. (1996) atlas, the *HST* QSO template of Zheng et al. (1997) as well as UV-optical spectrum of the metal-poor galaxy SBS 0335-052 with numerous strong optical emission lines (and an extinction of $E(B-V) \sim 0.09$; Izotov & Thuan 1998), kindly communicated to us by Yuri Izotov (private communication).

(ii) **BCCWW+**: Bruzual & Charlot (private communication; cf. Bruzual & Charlot 1993) evolving synthesis models assuming bursts, constant SF and exponentially decaying SF histories reproducing present day spectra of galaxies of various types (E, S0, Sa, Sb, Sc, Sd and Im) plus the empirical E, Sbc, Scd and Im templates from Coleman, Wu & Weedman (1980), as included in the public HYPERZ version.

(iii) **S03+**: theoretical templates of starburst galaxies from Schaerer (2003) covering metallicities of $Z = 0.02$ (solar), 0.008, 0.004, 0.001 and $1/50\,Z_{\odot}, Z = 10^{-5}, 10^{-7}$ and zero metallicity (PopIII). For low metallicities ($Z \leqslant 10^{-5}$), these templates have been computed for three different assumptions on the initial mass function (IMF). The spectral library includes burst models and models with a constant SFR. For more details see Schaerer (2003). For the present work these computations were extended to cover ages of up to 1 Gyr. These SEDs are available on request from the first author and on the Web.[2]

The standard extinction law adopted here is the one from Calzetti et al. (2000) determined empirically from nearby starbursts. We also explore the possible implications of other laws, such as the Galactic law of Seaton (1979) including the 2200-Å bump, and the Small Magellanic Cloud (SMC) law from Prévot et al. (1984) and Bouchet et al. (1985) showing no UV bump, but a steeper increase of the extinction in the UV compared to Calzetti et al.

For the Lyman forest attenuation, HYPERZ follows Madau (1995). However, we allow for possible deviations from the mean attenuation by varying the Lyman forest optical depths $\tau_{\rm eff}^{\alpha,\beta}$ by a multiplicative factor taking the values of ($f_{\rm Lyf}$, 1. and $1/f_{\rm Lyf}$). Typically, we adopted $f_{\rm Lyf} = 2$ or 3. Here $\tau_{\rm eff}^{\alpha,\beta}$ stands for the optical depths corresponding to the absorption between Lyα and Lyβ, and between Lyβ and the Lyman limit, respectively.

The following other minor changes have been made in our version (1.3ds) of HYPERZ. The calculation of the synthetic photometry

[2] http://obswww.unige.ch/sfr

deals correctly with templates including strong spectral lines (emission or absorption). Furthermore, we make sure to use the proper filter transmission curves usually given in photon units. Earlier versions of HYPERZ and other codes (e.g. evolutionary synthesis codes) assume sometimes (for 'historical' reasons) that transmission curves be given in flux units. In case of wide filters, for example, such as some ACS/*HST* filters, this may lead to small differences. Other modifications concern essentially features related to the user interface (additional outputs, etc.).

For given choices of the above parameters, the HYPERZ code performs a standard minimization fit to the observed SEDs and determines, for each point in the parameter space, the corresponding χ^2 value. Using these χ^2 values, it is possible to quantify the probabilities for the main free parameters, namely extinction, age of the spectral template, SF history, etc. When the SED fitting is based on theoretical templates, the SFR value is easily obtained and allows us to compare the expected values for the Lyα flux to the actual ones.

To convert the observed/adjusted quantities to absolute values, we adopt the following cosmological parameters: $\Omega_{\rm m} = 0.3, \Omega_\Lambda = 0.7$, and $H_0 = 70$ km s^{-1} Mpc^{-1}.

4 RESULTS FOR ABELL 2218 KESR

4.1 Photometric redshift estimate

As a spectroscopic redshift has not been obtained (yet) for this galaxy, we here examine its photometric redshift estimate. In Fig. 2, we show the photometric redshift probability distributions $P(z)$ for the two SEDs (SED1 and SED2) of Abell 2218 KESR described above using the three spectral template groups and adopting a minimum photometric error of 0.15 mag. For each redshift, $P(z)$ quantifies the quality of the best-fitting model obtained varying all other parameters (i.e. extinction, $f_{\rm Lyf}$, spectral template among template group). Given the excellent *HST* (WFPC2, ACS and NICMOS) photometry, $P(z)$ is quite well defined: the photometric redshift ranges typically between $z_{\rm phot} \sim 5.5$ and 7.3. Outside of the plotted redshift range, $P(z)$ is essentially zero. If we assume the (smaller) quoted formal photometric errors (but note the discrepancies discussed in Section 2), $P(z)$ becomes more peaked, that is, the photometric redshift better defined. This is driven by the error on the $z_{\rm 850LP}$ flux, which determines the red side of the Lyα break. However, the resulting best-fitting value $z_{\rm phot}$ does not change much. Furthermore, the fit quality is considerably decreased. This demonstrates the interest of such high accuracy measurements and the need for reliable error estimates.

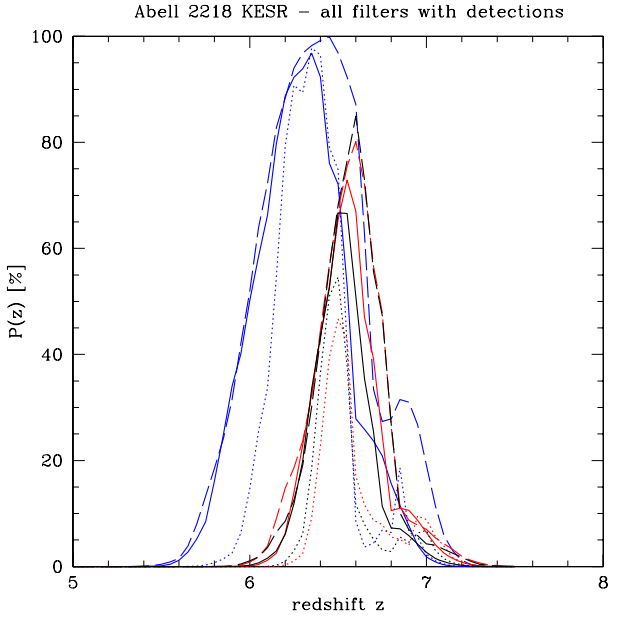

Figure 2. Photometric redshift probability distributions $P(z)$ of Abell 2218 KESR using three spectral template groups. Solid line: BCCWW+ template group; dotted: SB+QSO; long dashed: S03+. The three upper blue curves stand for the average SED of a and b (SED1), and the lower red ones for the SED of object b (SED2) from Egami et al. (2005). In all cases, a minimum photometric error of 0.15 mag was adopted. The $P(z)$ shown here has been computed based on all filters in which the object is detected ($I_{\rm 814W}$ to 4.5 μm).

The predicted redshift distribution is found to be quite insensitive to the exact template (as shown in Fig. 2), to the exact value of $f_{\rm Lyf}$ and to the adopted extinction law (variations of the latter two are not shown). However, we note that for this object the fits (and $P(z)$) are improved when allowing for deviations from the average Madau (1995) attenuation law. The curves shown here have been computed for $f_{\rm Lyf} = 2$.

More important in determining $P(z)$ is the exact SED. As seen from Fig. 2, the use of SED1 or SED2 leads to somewhat different $P(z)$ distributions. SED2 (cf. Section 2) yields a somewhat larger redshifts, albeit with a somewhat reduced fit quality. These differences illustrate how uncertainties and difficulties in the photometric measurements of such faint sources, whose origins are briefly discussed in Section 2, propagate to the photometric redshift estimate.

All our best-fitting solutions have redshift $z_{\rm phot} \sim 6.25$–6.63, lower than the redshift range estimated by KESR, but compatible with the more recent quantitative analysis of Egami et al. (2005). Given the various free parameters, uncertainties on the intrinsic SED, etc., we conclude that the redshift of Abell 2218 KESR is likely $z \sim 6.0$–7.2, taking into account both our photometric determination and the lensing considerations of KESR.

4.2 SED fits and inferences on the stellar population and on Lyα

A large number of models have been computed using the different variants of the SEDs describing this object (SED1–2), the different filter combinations (non-detections + spectroscopic constraint) discussed in Section 2, and varying the various model parameters. We first discuss briefly the main salient results with the help of some illustrations. A more general discussion of the results and their dependence on various assumptions follow.

4.2.1 Age, star formation history and extinction

Fig. 3 shows the best-fitting models to the SED2 including the upper limits from the $I_{\rm 814W}$ and LRIS spectroscopy for the S03+ and SB+QSO template groups. The best-fitting redshifts are $z_{\rm phot} = 6.63$ and 6.54, respectively. These fits show in particular that the spectroscopic constraint can be accommodated simultaneously with the observed $z_{\rm 850LP}$ flux; the resulting fits are within the 1σ errors in all bands. The best fit from the S03+ group corresponds to a burst with an age of 15 Myr at solar metallicity and no extinction (solid line). Similarly, good fits are also obtained for lower metallicity. The best fit with empirical starburst and QSO templates (SB+QSO)

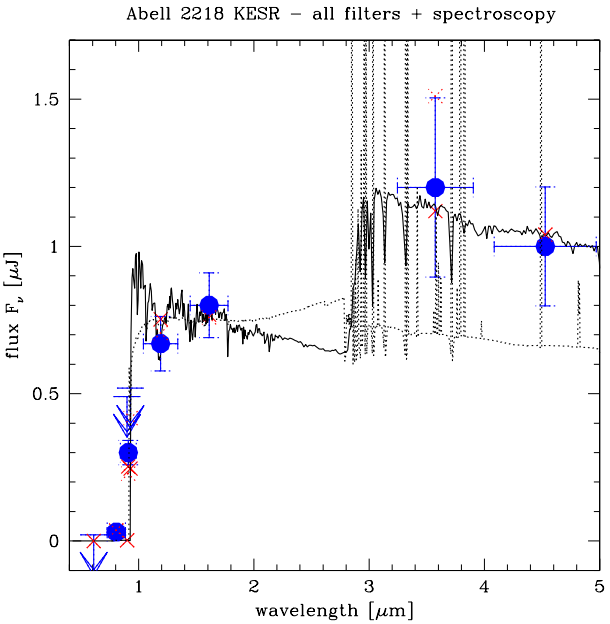

Figure 3. Best-fitting SEDs to the observations of Abell 2218 (SED2 from Egami et al. 2005, including the flux limit from the non-detections in V_{606W} and at 9000–9300 Å from spectroscopy; cf. Section 2). The red crosses indicate the corresponding model broad-band fluxes. The solid line shows the best fit for a template from the S03+ group, and dotted from the SB+QSO group. The redshifts for these solutions are $z \sim 6.63$ and 6.54, respectively. See text for more information.

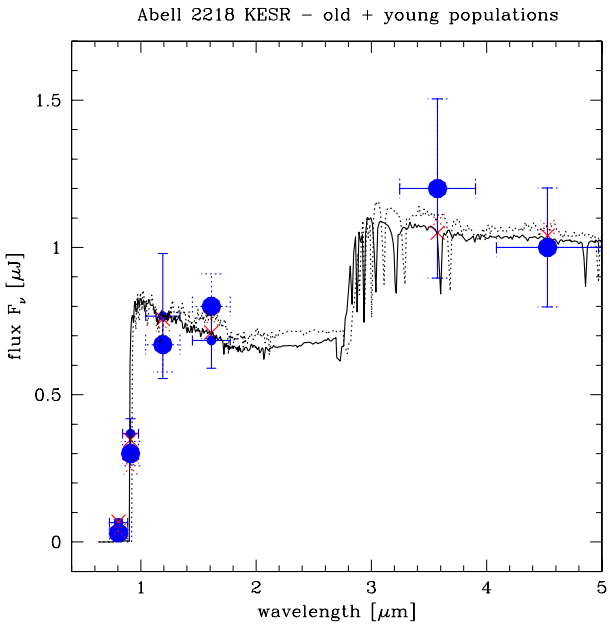

Figure 4. Best-fitting SEDs to the observations of Abell 2218 (Large symbols: SED2 from Egami et al. 2005; small symbols: SED1; cf. Section 2). Only true detections are taken into account. The red crosses indicate the corresponding model broad-band fluxes. The solid (dotted) line shows the best fit for a template with constant SFR from the S03+ group to the SED1 (SED2). The best 'maximum age' fits correspond to ages of 500 and 400 Myr, no extinction and redshifts $z_{\rm phot} \sim 6.40$ and 6.57, respectively, for SED1 and SED2. See text for more information.

is obtained with the spectrum of the metal-poor H II galaxy SBS 0335-052 (dotted line in Fig. 3). In this case, the apparent Balmer break observed between the NICMOS/*HST* and IRAC/*Spitzer* domain is simply explained by the presence of strong emission lines in the 3.6- and 4.5-μm filters[3] and some additional extinction to reduce the rest-frame UV flux. The extinction needed is $A_V = 0.6$ for the Calzetti et al. law, or $A_V = 0.2$ for the Prévot et al. extinction law. In terms of age, the rest-frame UV to optical spectrum (continuum and lines) of SBS 0335-052 corresponds to a young population of ∼3–5 Myr according to the analysis of Papaderos et al. (1998) and Vanzi et al. (2000). Of course, the presence of an older population in addition to the starburst cannot be excluded on the present grounds. In short, the observed SED of Abell 2218 KESR can be explained by a young population without or with emission lines. Spectroscopy in the 3–4 μm range would be needed to distinguish the latter solution from others.

Alternatively, good SED fits are also obtained with relatively 'old' populations. The oldest ages are obtained when invoking the longest SF time-scale, that is, constant SF. In this case, the UV rest-frame flux remains high (due to the continuous formation of massive stars) and older ages need to be attained to build up a sufficient population of evolved stars with strong Balmer breaks, in order to reproduce the observed break. This case is shown in Fig. 4 with fits with the S03+ templates to the observed SED1 and SED2. The best-fitting solutions obtained here correspond to ages of 500 and 400 Myr, no extinction, and redshifts $z_{\rm phot} \sim 6.40$ and 6.57, respectively. Similar, but somewhat older ages are obtained for metallicities $Z < 0.008$, below the ones shown here.

A quantitative examination of the 'maximum age' allowed by the observations (here SED2) is presented in Fig. 5, showing χ^2 contours in the extinction – age plane for a given set of spectral templates (S03+ group with constant SFR), the Calzetti et al. extinction law and a fixed redshift of $z = 6.55$. For these conditions, the best fit corresponds to 400 Myr, zero extinction and $z_{\rm phot} = 6.57$ (see Fig. 4). This figure shows that a maximum age of ∼250–650 Myr (1σ interval) is obtained, in good agreement with the modelling of Egami et al. (2005). If true, this would correspond to a formation redshift of $z_{\rm form} \sim 8.7$–20 for our adopted cosmological parameters. As clear from Fig. 5, even with constant SF models, younger populations with some extinction can also fit, although less well, the present observations. However, solutions with low or zero extinction are generally preferred.

When varying the SF history between these extreme cases (burst or SFR=constant), that is, considering, for example, exponentially declining SF histories, any intermediate age can be found for obvious reasons. Such cases are, for example, obtained when fitting templates from the Bruzual & Charlot models (not shown here) with exponentially decreasing SF histories and can be found in Egami et al. As discussed in Section 3.1, considering multiple stellar populations (cf. Eyles et al. 2005) does not alter the above estimate of the maximum age determined from constant SFR models. In any case, the data available here do not allow us to constrain the SF history and age further.

4.2.2 Lyα emission

The observations obtained so far have not revealed any emission line from this object (KESR). In particular, Lyα emission is lacking,

[3] The main lines are between Hγ, Hβ and [O III] λλ4959, 5007 in the 3.6-μm filter and He I λ5876 in the 4.5-μm filter. For example, for the emission lines between Hγ and [O III] λλ4959, 5007 the total observed equivalent width (boosted by the $(1 + z)$ factor) is ∼9130 Å, as estimated from the data of Izotov & Thuan (1998), compared to a filter surface of ∼6600 Å.

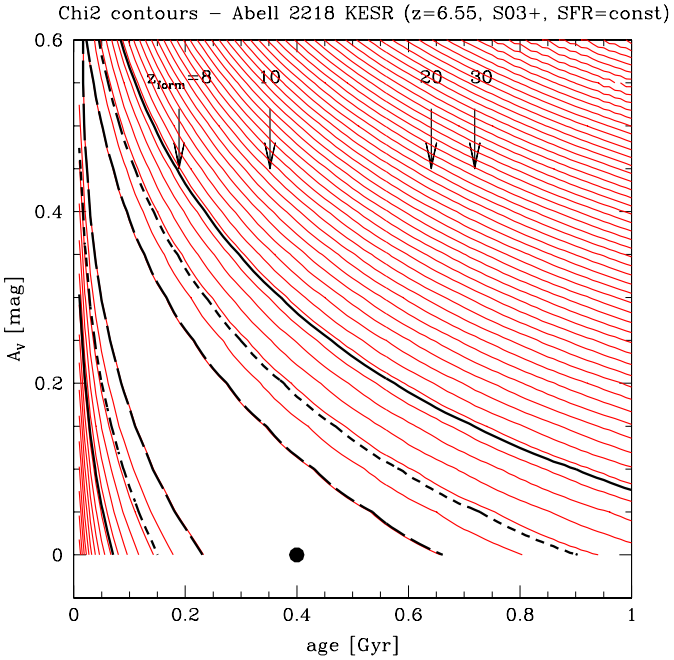

Figure 5. χ^2 contour plot in extinction – age for solutions fitting the observed SED2 at redshift $z = 6.55$ with templates from the S03+ group assuming constant SF. The best-fitting solution is indicated by the black dot. Equidistant χ^2 levels with a spacing of one are shown. The (1D) 68, 90 and 99 per cent confidence regions ($\Delta\chi^2 = 1$, 2.71, 6.63) are delimited by the thick black lines in long dashed, dotted and solid, respectively. Corresponding formation redshifts $z_{\rm form}$ (assuming the cosmological parameters given in Section 3.2) are indicated by the arrows. Discussion in text.

which could be puzzling for a source with intense SF. As we have just seen a variety of SF histories and ages are possible for Abell 2218 KESR. Therefore, one may or may not expect intrinsic Lyα emission.

A simple explanation for the apparent absence of Lyα emission could be to invoke an advanced age (in the post-starburst phase). However, even with a young age, it is not necessary that Lyα emission be observed. For example, the spectrum of the metal-poor H II galaxy SBS 03335-052 which provides an excellent fit to the observed SED and shows strong emission lines (cf. Fig. 3) does not show Lyα emission (Thuan, Izotov & Lipovetsky 1997; Kunth et al. 2003). Alternatively, if intrinsically present, the Lyα non-detection could be due to a variety of factors: a redshift $z \lesssim 6.4$ placing Lyα below the spectral range discussed in detail by KESR,[4] a flux below their strongly varying detection threshold, or other factors depressing the Lyα emission within the host galaxy (dust, ISM+HI geometry) and in the intervening IGM.

In conclusion, from the available data the apparent lack of Lyα emission from this source is not puzzling. However, it is not completely excluded that the galaxy truely shows Lyα emission, which has so far eluded detection.

4.2.3 General comments on fits and discussion

After these main findings we will now quickly mention more 'technical' results about the influence of various fit parameters.

[4] This is probably excluded as, according to J.-P. Kneib (private communication), no emission line was found in the blue part of the spectrum taken with LRIS.

Quite generally, the results on the age, SF history, extinction, etc. depend little on the different variants of the observed SEDs (SED1–2), on the inclusion or not of the non-detections in the fits, and on the use of the published formal errors or a minimum error of 0.15 mag (cf. Section 2). The results discussed above are therefore quite robust with respect to these assumptions. Small differences in the best-fitting values can, however, be obtained. For example, the best-fitting photometric redshift can vary by up to $\lesssim$0.2 depending on adopting SED1 or SED2. In all cases, we note that SED1 allows better fits (smaller χ^2) than SED2. Adopting $\sigma_{\rm min} = 0.15$ mag also significantly increases the fit quality. Finally, considering variations around the mean Lyman-forest attenuation improves the fits (especially as the *HST* photometry determining the Lyα break is quite accurate). In practice, all best fits are found with an increased Lyman forest opacity ($f_{\rm Lyf} = 2$).

To summarize, given the absence of a spectroscopic redshift, a fair number of good fits is found to the observations of Abell 2218 KESR when considering all the free parameters. The main conclusions from these 'best fits' are as follows.

(i) Generally, the determined extinction is negligible or zero quite independently of the adopted extinction law. The best fit with the empirical starburst spectrum of SBS 0335-052 represents an exception to this case, requiring an additional $A_V \sim 0.2$–0.6 mag, depending on the adopted extinction law.

(ii) Although generally burst models fit somewhat better than those with constant SF among the theoretical templates (BC, S03+), the data do not strongly constrain the SF history.

(iii) Typical ages between ∼15 and 400 Myr are obtained. A reasonable 1σ upper bound on the age of ∼650 Myr can be obtained assuming constant SF. However, the data can also be well fitted with a very young (∼3–5 Myr) stellar population with strong emission lines (using e.g. the spectrum of the metal-poor galaxy SBS 0335-052). In this case, the apparent Balmer break observed between the *HST* and *Spitzer* broad-band photometry is simply due to the presence of strong emission lines affecting the red 3.6- and 4.5-μm filters.

(iv) Given degeneracies of the rest-frame UV spectra between age and metallicity (cf. above), no clear indication on the galaxian metallicity can be derived, in contrast to the claim of KESR. Good fits to the available data can even be found with solar metallicity starburst templates.

(v) Depending on the SF history and age, one may or may not expect intrinsic Lyα emission, that is, an important H II region around the object. The apparent absence of the observed Lyα emission therefore does not provide much insight.

A more complete error analysis beyond the level presented here is difficult to achieve for a variety of reasons and clearly beyond the scope of this publication.

4.2.4 SFR, stellar mass and luminosity

The theoretical templates can also be used to estimate the stellar mass involved in the starburst or the SFR when constant SF is assumed. For this aim we use all the best fits to the three SEDs (SED1–3) with the S03+ templates, we assume a typical redshift of $z = 6.6$, and the magnification $\mu = 25$ is determined by KESR. For the adopted cosmology, the distance luminosity is then $d_{\rm L} = 64\,457.8$ Mpc.

When constant SF is assumed, one obtains the following SFR: SFR $\sim$ (0.9–1.1) $M_\odot$ yr^{-1} (for a Salpeter IMF from 1 to 100 $M_\odot$).

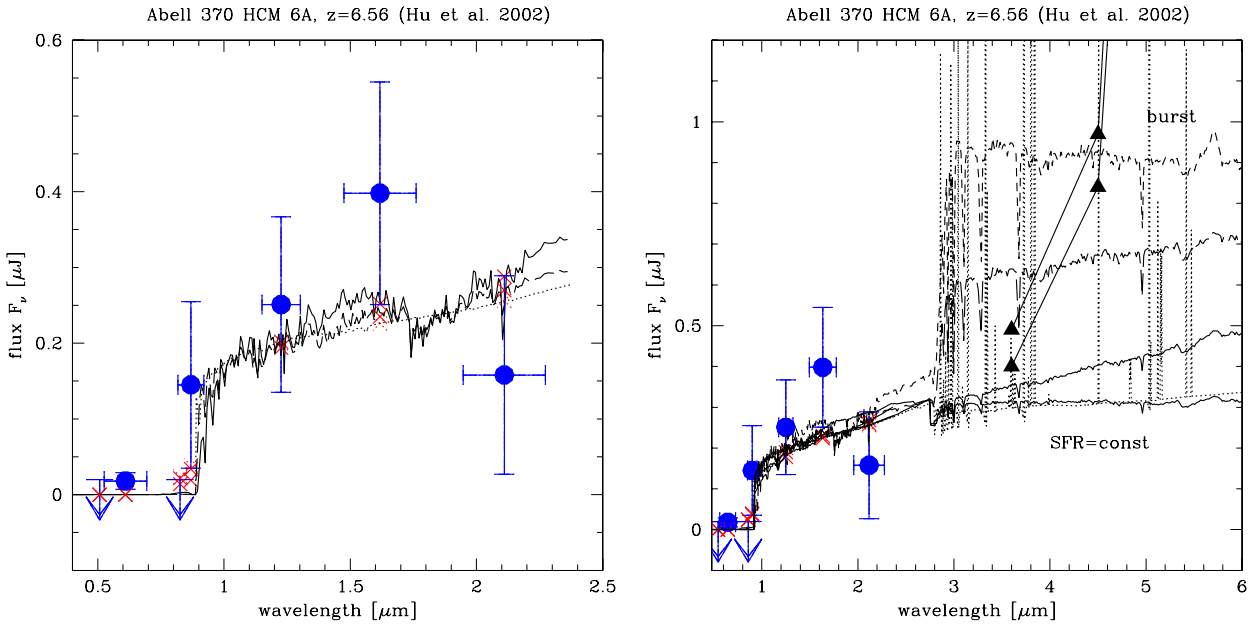

Figure 6. Best-fitting SEDs to the observations of Abell 370 HCM 6A. The red crosses indicate the corresponding model broad-band fluxes. Solid lines show the best fit for a template from the BC+CWW group, dotted from SB+QSO group, and dashed from the S03+ group (see explanations in Section 3). Left: observed spectral range. Right: predicted SED in *Spitzer*/IRAC domain for best-fitting models. Dashed lines show the bursts from the BCCWW+ and S03+ template groups. The dotted line is the spectrum of SBS 0335-052 from the SB+QSO group with additional $A_V = 1$. The solid lines show best fits for constant SF using different extinction/attenuation laws (Calzetti starburst law versus SMC law). The solid triangles illustrate the IRAC point-source sensitivity (1σ) for low and medium backgrounds excluding 'confusion noise'.

For the best-fitting ages of ∼400–570 Myr, the total mass of stars formed would then correspond to $\sim (3.6\text{–}6.3) \times 10^8\,\mathrm{M}_\odot$. The mass estimated from the best-fitting burst models (of ages ∼6–20 Myr) is slightly smaller, $M_\star \sim (0.3\text{–}1) \times 10^8\,\mathrm{M}_\odot$. If we assume a Salpeter IMF with $M_{\rm low} = 0.1\,\mathrm{M}_\odot$, the mass and SFR estimates would be higher by a factor of 2.55, and in good agreement with the values derived by KESR and Egami et al. (2005). In all the above cases, the total luminosity (unlensed) is typically $L_{\rm bol} \sim 2 \times 10^{10}\,\mathrm{L}_\odot$.

5 RESULTS FOR ABELL 370 HCM 6A

5.1 SED fits and inferences on the stellar population

Overall, the published SED of HCM 6A (see Fig. 6) is 'reddish', showing an increase of the flux from Z to H and even to K'.[5] From this simple fact and the above explanations it is already clear qualitatively that one is driven towards solutions with (i) 'advanced' age and little extinction or (ii) constant or young SF plus extinction. However, (i) can be excluded as no Lyα emission would be expected in this case.

Quantitatively, the best solutions obtained for each spectral template group are shown in the left panel of Fig. 6. Indeed, the solutions shown correspond to bursts of ages ∼50–130 Myr (BCCWW+, S03 templates) and little or no extinction. However, as just mentioned, solutions lacking young ($\lesssim$10 Myr) massive stars can be excluded since Lyα emission is observed. The best-fitting empirical SB+QSO template shown corresponds to the spectrum of the H II galaxy SBS 0335-052 with an additional extinction of $A_V = 1$. To reconcile the observed SED with Lyα, a young population, for example, such as SBS 0335-052, or constant SF is required. In any of these cases, fitting the 'reddish' SED requires a non-negligible amount of reddening.

To illustrate the typical range of possible results, we show in Fig. 7 χ^2 contour maps and corresponding confidence intervals for solar metallicity models (S03+ template group) and reddened with the Calzetti law. The left-hand panel (burst models) illustrates in particular the need for progressively higher extinctions the younger the bursts. Models with ages $\gtrsim$10 Myr are excluded for the absence of Lyα emission. From the constant SF models (right-hand panel), we see that for a given age A_V is typically ∼0.5–1.8 mag at the 68 per cent confidence level. For obvious reasons, no constraint can be set on the age since the onset of (constant) SF.

Hence, from the photometry of HCM 6A and from the presence of Lyα we are led to conclude that this object must suffer from reddening with typical values of $A_V \sim 1$. for a Calzetti attenuation law. A somewhat smaller extinction ($A_V \sim 0.4$) can be obtained if the steeper SMC extinction law of Prévot et al. (1984) is adopted. From the present data, it is not possible to distinguish the different extinction/attenuation laws. Also, it is not possible to draw any constraint on the metallicity of HCM 6A from the available data (cf. Section 3.1).

What if we are dealing with composite stellar populations? Indeed, it is conceivable that the Lyα emission originates from a population of young stars and the 'reddish' rest-frame UV flux be due to another, older population. Assuming constant SF, no loss of Lyα and standard SFR conversion factors, the observed Lyα emission implies a maximum UV flux of the order of 0.1 μJy (and approximately constant in F_ν over the observed wavelength range: $\lambda_{\rm rest} \gtrsim$ 3000 Å) for an unreddened population. The bulk of the observed flux could then be from an older population. In this case, the rising spectrum from the $z_{850\mathrm{LP}}$ over the JH (and presumably K) bands could even be due to an unreddened population; a strongly increasing

[5] The significance of a change in the SED slope between ZJH and HK' seems weak, and difficult to understand.

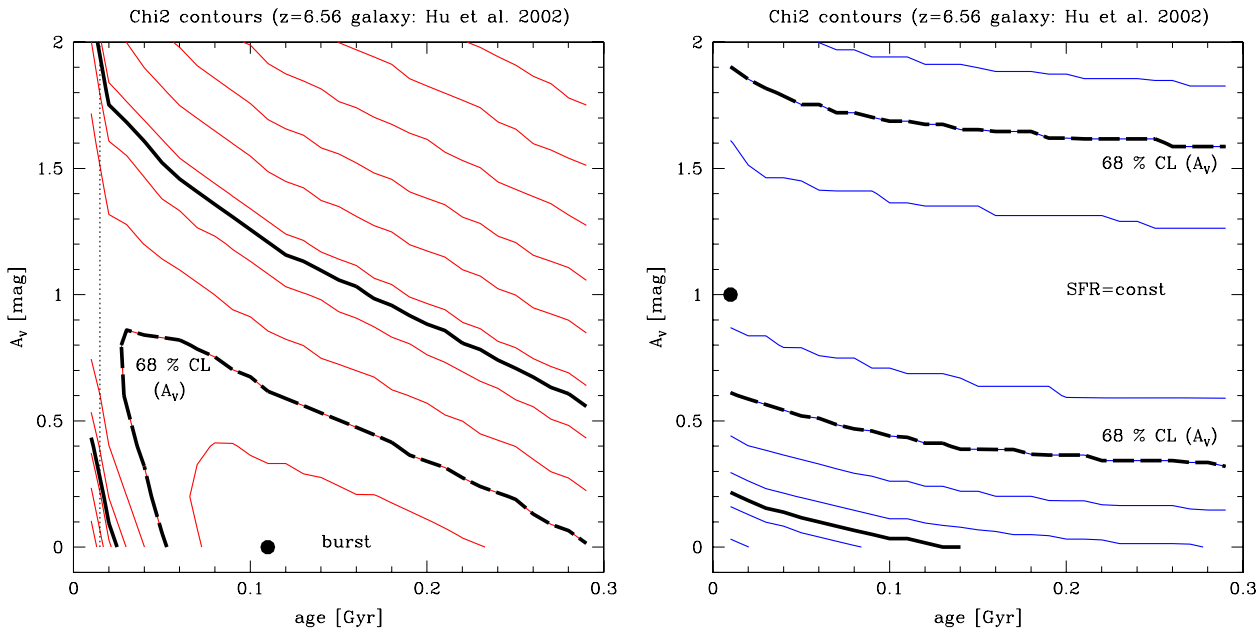

Figure 7. χ^2 contour plots showing solutions in extinction – age diagrams. The best solutions are indicated by the black dot. Equidistant χ^2 levels with a spacing of 0.5 are shown. The 2D 68 per cent confidence region (corresponding to $\Delta\chi^2 = 2.3$) is delimited by the solid thick black line. The (1D) 68 per cent confidence region for A_V ($\Delta\chi^2 = 1.$) at each given age is delimited by the dashed thick black line. Left: plot for solutions using a solar metallicity burst template from the S03+ template group and the Calzetti attenuation law. Although providing a good fit to the photometry, the region corresponding to ages $\gtrsim$15 Myr, right of the dotted vertical line, is excluded as no emission line would be expected in this case. Right: same as left-hand panel for constant SF models. The solutions indicate a non-negligible extinction, but no constraint on age. Discussion in text.

flux and probably a significant 'Balmer' break is then expected, similar to the aged burst shown in the right panel of Fig. 6. This explanation should in principle be testable with *Spitzer* observations as discussed below.

How does our possible indication for a high extinction fit in with other studies? At redshift $z \lesssim 4$, the extinction of Lyman break galaxies (LBGs) has been estimated by various authors (e.g. Sawicki & Yee 1998; Meurer, Heckman & Calzetti 1999; Adelberger & Steidel 2000; Shapley et al. 2001; Ouchi et al. 2004). Given their mean/median values (typically $\langle E(B-V)\rangle \sim 0.15$–$0.2$) and the $E(B-V)$, our finding of a 'high' extinction is not exceptional. Furthermore, Armus et al. (1998) find indications for $A_V > 0.5$ mag from their analysis of a $z = 5.34$ galaxy. However, this implies that dust extinction is likely to be present in starburst galaxies with redshifts above six. Large amounts of dust have already been observed in QSOs up to similar redshift (Bertoldi et al. 2003; Walter et al. 2003).

5.2 Properties of HCM6A: SFR, mass and Lyα transmission

To estimate properties such as the mass, SFR and the intrinsic Lyα emission from HCM 6A, we simply examine the predictions from the best-fitting models, scale them appropriately to the luminosity distance,[6] and correct for the gravitational magnification (here $\mu = 4.5$). The derived quantities are summarized in Table 1.

First, we consider single (non-composite) stellar populations. From the best-fitting constant SF models (with variable ages), we deduce an extinction-corrected SFR of the order of SFR(UV) $\sim$11–41 $M_\odot$ yr^{-1} for a Salpeter IMF from 1 to 100 $M_\odot$. For a commonly adopted, although unjustified, Salpeter IMF down to 0.1 $M_\odot$ this would increase by a factor of 2.55. Actually this estimate is not very different than the one obtained from standard SFR calibrations, provided the same assumptions on the IMF. Indeed, the observed rest-frame UV luminosity, for example, derived from the average J, H and K' flux of $F_{\rm UV} = (2.6 \pm 0.7) \times 10^{-30}$ erg s^{-1} cm^{-2} Hz^{-1} is $L_{\rm restUV} = 4\pi d_{\rm L}^2 F_{\rm UV}/(1+z)/\mu \approx 4. \times 10^{28}$ erg s^{-1} Hz^{-1} (Hu et al. 2002) translates to SFR$_{\rm UV} \approx c\, L_{\rm restUV}\, 10^{0.4 A_{\rm UV}}$, where c is the usual SFR conversion coefficient and $A_{\rm UV}$, the UV extinction. For the standard value $c = 1.4 \times 10^{-28}$ from Kennicutt (1998), assuming a Salpeter IMF down to 0.1 $M_\odot$ and $A_{\rm UV} \sim 2.0$–3.0, one has SFR $\sim$ 35–88 $M_\odot$ yr^{-1}; for the IMF used in this work (Salpeter from 1–100 $M_\odot$), this becomes SFR $\sim$ 14–34 $M_\odot$ yr^{-1}. This assumption and the absence of extinction correction also explain the difference with SFR estimate of Hu et al. (2002).[7]

For continuous SF over time-scales, $t_{\rm SF}$ longer than $\sim$10 Myr, the total (bolometric) luminosity output is typically $\sim 10^{10}$ $L_\odot$ per unit SFR (in $M_\odot$ yr^{-1}) for a Salpeter IMF from 1 to 100 $M_\odot$, quite independently of metallicity. The total luminosity associated with the observed SF is therefore $L \sim$ (1–4) $\times 10^{11}$ $L_\odot$, close to or just above the limit to possibly qualify as a luminous infrared galaxy ($L_{\rm IR} > 10^{11}$ $L_\odot$; cf. Sanders & Mirabel 1996), if a significant fraction of its bolometric flux emerges in the (rest frame) IR. For $t_{\rm SF} \sim$ 10 Myr the estimated stellar mass is $M_\star \approx t_{\rm SF} \times$ SFR $\sim$ (1–4) $\times$ 10^8 $M_\odot$.

From the data given by Hu et al. (2002), the observed Lyα flux is $F(\mathrm{Ly}\,\alpha) = \mu \times 3.8 \times 10^{-18}$ erg s^{-1} cm^{-2}, with the magnification

[6] For the adopted cosmology and $z = 6.56$, one has $d_{\rm L} = 640\,05.7$ Mpc.

[7] Actually Hu et al. (2002) derive without further explanation SFR = 9 $M_\odot$ yr^{-1} from $L_{\rm restUV} = 4. \times 10^{28}$ erg s^{-1}, whereas the classical Kennicutt (1998) calibration would yield SFR = 5.6 $M_\odot$ yr^{-1} without extinction correction.

factor μ. The Lyα luminosity per unit SFR from the same S03 models used above is $L(\mathrm{Ly}\alpha) = (2.4\text{–}4.4) \times 10^{42}\,\mathrm{erg\,s^{-1}}\,(\mathrm{M_\odot\,yr^{-1}})^{-1}$ for metallicities between solar and $1/50\,\mathrm{Z_\odot}$. The SFR deduced from Lyα would then be SFR (Lyα) $\sim$ 0.4–0.8 $\mathrm{M_\odot\,yr^{-1}}$ for HCM 6A. Taking an extinction of $A_V = 1.$ (for the Calzetti law) into account implies a reddening corrected SFR (Lyα) $\sim$ 7–12 $\mathrm{M_\odot\,yr^{-1}}$. The ratio between SFR(Lyα) and SFR(UV) presumably reflects the incomplete Lyα transmission $t_{\mathrm{Ly}\alpha}$, which can be estimated in various ways. The most consistent estimate is obtained from the comparison of the predicted Lyα luminosity of each best-fitting model (obtained from fitting the broad-band SED) to the observed Lyα luminosity. From the best-fitting models with $A_V \sim 1$ and the Calzetti law, we obtain $t_{\mathrm{Ly}\alpha} \sim$ 23–54 per cent; in the case of the fit with the Prévot et al. extinction law, we find a higher transmission $t_{\mathrm{Ly}\alpha} \sim 90$ per cent. For comparison, Haiman (2002) assumed a Lyα transmission of 20 per cent from the data of Hu et al. Per definition this Lyα 'transmission' corresponds to the ratio of the expected/intrinsic Lyα emission from the starburst over the observed one. The physical causes for a partial (i.e. <100 per cent) transmission are of course open to various interpretations (e.g. physical processes destroying Lyα photons in the host galaxy, absorption in the intervening IGM, etc.). In fact the relatively high Lyα transmission estimated here could be somewhat surprising, given the Gunn–Peterson trough observations in $z \gtrsim 6$ quasars (cf. Becker et al. 2001; Fan et al. 2003) and the possible presence of dust (this work).

Consider now the case of composite stellar populations. In this case, we retain as a rough estimate in Table 1 the SFR(Lyα) (from the young population) as a lower limit, and the mass and total luminosity is derived from the best-fitting burst model of age $\sim$100 Myr assuming that this 'older' population dominates the observed continuum flux. Formally, we then have no handle on the Lyα transmission, except that it cannot be very low (say $\lesssim$40 per cent $\approx 0.1/0.26 = F_{\mathrm{young}}/\langle F_{\mathrm{obs}}\rangle$) since otherwise the associated UV flux from the young population F_{young} would dominate the observed continuum flux $\langle F_{\mathrm{obs}}\rangle$.

5.3 *Spitzer* observatory predictions

It is interesting to examine the SEDs predicted by the various models at longer wavelengths, including the rest-frame optical domain, which is potentially observable with the sensitive IRAC camera onboard the *Spitzer* observatory and other future missions. In the right panel of Fig. 6, we plot the three best fits to the observed data for the BCCWW+ and S03+ template groups ('burst' solutions with no extinction) and the SBS 03352-052 template (with additional $A_V = 1$) showing strong optical emission lines. We see that these solutions have fluxes comparable to or above the detection limit of IRAC/*Spitzer*.[8] On the other hand, the strongly reddened constant SF or young burst solutions do not exhibit a Balmer break and are hence expected to show fluxes just below the IRAC sensitivity at 3.6 μm and significantly lower at longer wavelengths. As Lyα emission is expected only for the reddened SEDs, the latter solutions (low 3.6–4.5 μm flux) are predicted to apply to HCM 6A, except if composite stellar populations are considered. Indeed, a high 3.6- and 4.5-μm flux could be a good indication for a composite stellar population, as discussed above. In addition, it is important to secure higher accuracy photometry especially in the near-IR (*JHK*) to assess the accuracy of the redward increasing shape of the spectrum (in F_ν), which drives one towards solutions with non-negligible extinction.

[8] The IRAC detection limits plotted here correspond to the values given by the Spitzer Science Centre http://ssc.spitzer.caltech.edu/irac/sens.html as 1σ point-source sensitivity for low and medium backgrounds for frame times of 200 s and described by Fazio et al. (2004). These values do not include 'confusion noise'.

6 CONCLUSION

Using SED fitting techniques considering a large number of parameters (mainly a vast library of empirical and theoretical template spectra, variable extinction and extinction laws), we have attempted to constrain the properties of the stellar populations and Lyα emission of two strongly lensed galaxies with redshifts $z \gtrsim 6$ from their observed SED including various ground-based observations, *HST*, and *Spitzer* observations.

The following main results have been obtained for these objects (see Sections 5 and 4 and summary in Table 1).

(i) **Triple arc in Abell 2218** discovered by KESR. The most likely redshift of this source is $z \sim 6.0$–7.2, taking into account both our photometric determination and lensing considerations.

SED fits indicate generally a low extinction ($E(B-V) \lesssim 0.05$) but do not strongly constrain the SF history. Best fits have typical ages of $\sim$3 to 400 Myr. A reasonable maximum age of 250–650 Myr (1σ interval) can be estimated. However, the apparent 4000-Å break observed recently from combination of IRAC/*Spitzer* and *HST* observations, can also equally well be reproduced with the template of a young ($\sim$3–5 Myr) burst where strong rest-frame optical emission lines enhance the 3.6- and 4.5-μm fluxes.

The estimated SFR is typically $\sim 1\,\mathrm{M_\odot\,yr^{-1}}$ for a Salpeter IMF from 1 to 100 $\mathrm{M_\odot}$, in agreement with previous estimates.

Given the poor constraint on age and SF history, we conclude that intrinsic Lyα emission may or may not be present in this galaxy. The apparent non-detection of Lyα by KESR can therefore even be understood without invoking Lyα destruction.

(ii) **Abell 370 HCM 6A** discovered by Hu et al. (2002). The relatively red SED and the presence of Lyα emission indicate basically two possible solutions: (1) a young burst or an ongoing constant SF with non-negligible extinction ($A_V \sim 0.5$–1.8 at a 1σ level or 2), a composite young + 'old' stellar population.

For the first case, the best fits are obtained for constant SF with $E(B-V) \sim 0.25$. In consequence, previous SFR estimates for this source must likely be revised upward. If correct, the bolometric luminosity of this galaxy is estimated to be $L \sim (1-4) \times 10^{11}\,\mathrm{L_\odot}$, comparable to the luminosity of infrared luminous galaxies. Furthermore, an Lyα transmission of $\sim$23–90 per cent is estimated from our best-fitting models.

Alternatively, the observed 0.9–2.2 μm SED could also be fit without extinction by a composite 'young' and 'old' stellar population, where the former would be responsible for the Lyα emission and a fraction of the rest-frame UV flux. The SFR, stellar mass and total luminosity are then lower than in case 1. The two scenarios may be distinguishable with IRAC/*Spitzer* observations at 3.6 and 4.5 μm.

Given the limited observed spectral range, the present data do not allow to draw any firm constraints on the maximum age of the stellar population.

In general, it should also be noted that broad-band SED fits or measurements of the UV slope do not allow one to determine the metallicity of a star-forming galaxy from a theoretical point of view

and in terms of individual objects given important degeneracies (cf. Section 3.1).

The estimates of the Lyα transmissions presented here can in principle be used to constrain the intervening IGM properties, and therefore probe the reionization of the Universe.

Although the results obtained here from this exploratory study of just two lensed galaxies, the highest known redshift galaxies with photometric detections in at least three to four filters, cannot provide a general view on the SF and IGM properties at $z \gtrsim 6$, there is a good hope that the sample of such objects will considerably increase in the near future with the availability of large ground-based telescopes and sensitive space-borne observatories such as *Spitzer* and even more so with the planned James Webb Space Telescope.

ACKNOWLEDGMENTS

We thank an anonymous referee for critical comments, which helped to improve the paper. We thank Eichi Egami and Johan Richard for comments on the *HST* and *Spitzer* photometry of the arc in Abell 2218 KESR, Jean-Paul Kneib for information on Keck spectroscopy of this object, and Yuri Izotov for communicating spectra of metal-poor galaxies. Part of this work was supported by the Swiss National Science Foundation and the CNRS.

REFERENCES

Adelberger K. L., Steidel C. C., 2000, ApJ, 544, 218
Ajiki M. et al., 2003, AJ, 126, 2091
Armus L., Matthews K., Neugebauer G., Soifer B. T., 1998, ApJ, 506, L89
Barkana R., Loeb A., 2001, Phys. Rep., 349, 125
Becker R. H. et al., 2001, AJ, 122, 2850
Bertoldi F. et al., 2003, A&A, 409, L47
Bolzonella M., Miralles J.-M., Pelló R., 2000, A&A, 363, 476
Bouchet P., Lequeux J., Maurice E., Prevot L., Prevot-Burnichon M. L., 1985, A&A, 149, 330
Bremer M. N., Lehnert M. D., Waddington I., Hardcastle M. J., Boyce P. J., Phillipps S., 2004, MNRAS, 347, L7
Bruzual G., 1983, ApJ, 273, 105
Bruzual G., Charlot S., 1993, ApJ, 405, 538
Bunker A., Stanway E. R., Ellis R. S., McMahon R. G., 2004, MNRAS, 355, 374
Calzetti D., Kinney A. L., Storchi-Bergmann T., 1994, ApJ, 429, 582
Calzetti D., Armus L., Bohlin R. C., Kinney A. L., Koornneef J., Storchi-Bergmann T., 2000, ApJ, 533, 682
Charlot S., Fall M. S., 1993, ApJ, 415, 580
Coleman D. G., Wu C. C., Weedman D. W., 1980, ApJS, 43, 393
Cuby J.-G., Le Févre O., McCracken H., Cuillandre J.-C., Magnier E., Meneux B., 2003, A&A, 405, L19
Dawson S. et al., 2004, ApJ, 617, 707
Dey A. J. et al., 1998, ApJ, 498, 93
Dickinson M. et al., 2004, ApJ, 600, L99
Egami E. et al., 2005, ApJL, 618, L5
Eyles L. P., Bunker A. J., Stanway E. R., Lacy M., Ellis R. S., Doherty M., 2005, MNRAS, in press (doi:10.1111/j.1365-2966.2005.09434) (astro-ph/0502385)
Fan X. et al., 2003, AJ, 125, 1649
Fazio G. G. et al., 2004, ApJS, 154, 10
Gnedin N. Y., Prada F., 2004, ApJ, 608, L77
Haiman Z., 2002, ApJ, 576, L1
Heckman T. M., Robert C., Leitherer C., Garnett D. R., van der Rydt F., 1998, ApJ, 503, 646
Hu E. M., McMahon R. G., Cowie L.L., 1999, ApJ, 522, L9
Hu E. M., Cowie L. L., McMahon R. G., Capak P., Iwamuro F., Kneib J.-P., Maihara T., Motohara K., 2002, ApJ, 568, L75 (Erratum: ApJ, 576, L99)
Izotov Y. I., Thuan T. X., 1998, ApJ, 500, 188
Kauffmann G. et al., 2003, MNRAS, 341, 33
Kennicutt R. C. Jr., 1998, ARAA, 36, 182
Kinney A., Calzetti, D., Bohlin R. C., McQuade K., Storchi-Bergmann T., Schmitt H. R., 1996, ApJ, 467, 38
Kneib J. P., Ellis R. S., Santos M. R., Richard J., 2004, ApJ, 607, 697
Kodaira K. et al., 2003, PASJ, 55, L17
Kunth D., Mas-Hesse J. M., Terlevich E., Terlevich R., Lequeux J., Fall S. M., 1998, A&A, 334, 11
Kunth D., Leitherer C., Mas-Hesse J. M., Östlin G., Petrosian A., 2003, ApJ, 597, 263
Lehnert M. D., Bremer M., 2004, The Messenger, 115, p. 27
Leitherer C., Heckman T. M., 1995, ApJS, 96, 9
Madau P., 1995, ApJ, 441, 18
Malhotra S., Rhoads J. E., 2002, ApJ, 565, L71
Malhotra S., Rhoads J. E., 2004, ApJ, 617, L5
Mas-Hesse J. M., Kunth D., Tenorio-Tagle G., Leitherer C., Terlevich R. J., Terlevich E., 2003, ApJ, 598, 858
Meurer G. R., Heckman T. M., Leitherer C., Kinney A., Robert C., Garnett D. R., 1995, AJ, 110, 2665
Meurer G. R., Heckman T. M., Calzetti D., 1999, ApJ, 521, 64
Ouchi M. et al., 2004, ApJ, 611, 660
Papaderos P., Izotov Y. I., Fricke K. J., Thuan T. X., Guseva N. G., 1998, A&A, 338, 45
Papovich C. et al., 2004, ApJ, 600, L111
Prévot M. L., Lequeux J., Prevot L., Maurice E., Rocca-Volmerange B., 1984, A&A, 132, 398
Rhoads J. E., Malhotra S., 2001, ApJ, 563, L5
Rhoads J. E. et al., 2003, AJ, 125, 1006
Sanders D. B., Mirabel I. F., 1996, ARAA, 34, 749
Santos M. R., 2004, MNRAS, 349, 1137
Sawicki M., Yee H. K. C., 1998, AJ, 115, 1329
Schaerer D., 2002, A&A, 382, 28
Schaerer D., 2003, A&A, 397, 527
Schaerer D., Pelló R., 2005, in Wilson A. ed., ESA SP-577 The Dusty and Molecular Universe: A Prelude to Herschel and ALMA. ESA Publications Division, Noordwijk, p. 121
Seaton M., 1979, MNRAS, 187, 73
Shapley A. E. et al., 2001, ApJ, 562, 95
Sirianni M. et al. 2004, PASP, submitted
Spinrad H., 2003 in Mason J. W., ed., Astrophysics Update. Heidelberg, Springer, p. 155, (astro-ph/0308411)
Taniguchi Y., Shioya Y., Fujita S. S., Nagao T., Murayama T., Ajiki M., 2003, JKAS, 36, 123 (astro-ph/0306409) (Erratum: JKAS, 36, 283)
Taniguchi Y. et al., 2005, PASJ, 57, 165
Tenorio-Tagle G., Silich S. A., Kunth D., Terlevich E., Terlevich R., 1999, MNRAS, 309, 332
Thuan T. X., Izotov Y. I., Lipovetsky V. A., 1997, ApJ, 477, 661
Valls-Gabaud D., 1993, ApJ, 419, 7
Vanzi L., Hunt L. K., Thuan T. X., Izotov Y. I., 2000, A&A, 363, 493
Walter F. et al., 2003, Nat, 424, 406
Zheng W., Kriss G. A., Telfer R. C., Grimes J. P., Davidsen A. F., 1997, ApJ, 475, 469

This paper has been typeset from a TEX/LATEX file prepared by the author.